Available online at www.sciencedirect.com

ScienceDirect

Scripta Materialia 94 (2015) 44–47

Scripta MATERIALIA

www.elsevier.com/locate/scriptamat

Enhancement of strain-rate sensitivity and shear yield strength of a magnesium alloy processed by high-pressure torsion

In-Chul Choi,[a] Dong-Hyun Lee,[a] Byungmin Ahn,[b] Karsten Durst,[c] Megumi Kawasaki,[a,*] Terence G. Langdon[d,e] and Jae-il Jang[a,*]

[a]*Division of Materials Science and Engineering, Hanyang University, Seoul 133-791, Republic of Korea*
[b]*Department of Energy Systems Research, Ajou University, Suwon 443-749, Republic of Korea*
[c]*Department of Materials Science, TU Darmstadt, D-64287 Darmstadt, Germany*
[d]*Departments of Aerospace & Mechanical Engineering and Materials Science, University of Southern California, Los Angeles, CA 90089-1453, USA*
[e]*Materials Research Group, Faculty of Engineering and the Environment, University of Southampton, Southampton SO17 1BJ, UK*

Received 20 August 2014; revised 12 September 2014; accepted 14 September 2014
Available online 1 October 2014

A Mg–Zn–Zr alloy was processed by high-pressure torsion for up to 2 turns at room temperature to produce significant grain refinement together with enhanced plasticity and strength. Measurements were performed to determine the strain-rate sensitivity, shear yield strength and activation volume as a function of the processing conditions. The results suggest there is a significant contribution from grain boundary sliding to the flow process and the onset of plasticity is associated with heterogeneous dislocation nucleation.

Keywords: Grain boundary sliding; High-pressure torsion; Magnesium alloy; Strain-rate sensitivity; Yielding

Magnesium alloys have attracted much attention as structural materials for automotive, aerospace and electronics applications because of their very high strength-to-weight ratio. However, there are drawbacks to using Mg alloys due their low ductility at room temperature (RT) due to their hexagonal close-packed (hcp) structure which provides only a limited number of active slip systems and a consequent poor workability and formability. Among various strategies to overcome this deficiency [1], one attractive approach is grain refinement which can improve both strength and ductility.

To date, one of the most recognized methods for achieving excellent grain refinement in bulk metals is through the application of severe plastic deformation in procedures such as equal-channel angular pressing (ECAP) [2] and high-pressure torsion (HPT) [3]. In general, Mg alloys are generally processed by ECAP at relatively high temperatures in order to avoid segmentation and cracking caused by their limited ductility at low temperatures [4,5]. By contrast, processing by HPT introduces a high hydrostatic pressure so that undesirable cracking may be avoided even at RT [6]. By comparison with ECAP, HPT processing also has an advantage in producing higher plastic strains and hence smaller grain sizes [7]. During HPT, the equivalent von Mises strain imposed on the disk, ε_{eq}, is given by $2\pi Nr/(\sqrt{3}t)$, where r and t are the radius and thickness of the disk and N is the number of torsional revolutions [8]. Therefore, in HPT the strain varies locally across the disk and this contrasts with ECAP where the imposed strain is reasonably constant.

Extensive research has examined the evolution of microstructure and hardness of Mg alloys during HPT processing at both RT and elevated temperatures [6,9,10]. Nevertheless, there was no attempt to monitor the changes in strain-rate sensitivity, m, and shear yield strength, τ_y, of Mg alloys processed by HPT although these are essential parameters for estimating the workability of the alloys. The present research was motivated to address this deficiency by using nanoindentation to explore the evolution of m and τ_y and the activation volume, V^*, in a ZK60 Mg alloy. This alloy was selected because it has the best combination of strength and ductility at RT among the common wrought Mg alloys with principal alloying elements of Al, Mn and Zn [11].

An extruded ZK60 (Mg–5.5 Zn–0.5 Zr in wt.%) Mg alloy with a diameter of 10 mm was cut into disks

* Corresponding authors; e-mail addresses: megumi@hanyang.ac.kr; jijang@hanyang.ac.kr

http://dx.doi.org/10.1016/j.scriptamat.2014.09.014
1359-6462/

~1.5–2.0 mm thick and these disks were carefully polished on both sides to final thicknesses of ~0.8 mm. The HPT processing was conducted at RT under quasi-constrained conditions [12] using a pressure of 6.0 GPa, a rotational speed of 1 rpm and with the disks processed through $N = 1/4$, 1/2, 1 and 2 turns. After processing, the disks were mechanically polished to a mirror-like finish and then etched with a solution of 60 ml ethylene glycol, 20 ml glacial acetic acid, 19 ml distilled water and 1 ml nitric acid for the as-extruded sample and a solution of 1 g oxalic acid, 1 ml nitric acid and 98 ml distilled water for the processed specimens. The microstructures at the edges of the disks were examined using an optical microscope (CK40M, Olympus, Tokyo). The distributions of the Vickers microhardness, Hv, across the diameters of each disk were measured with HMV-2 equipment (Shimadzu, Tokyo) at a peak load P_{max} of 980 mN.

Three different nanoindentation tests were performed at the edge of each disk using a Nanoindenter-XP (formerly MTS; now Agilent, Oak Ridge, TN) which permits constant strain rate (CSR) testing, strain-rate jump (SRJ) testing and "pop-in" testing. The first two tests were performed with a three-sided pyramidal Berkovich indenter in order to estimate m. The pop-in tests were conducted with a spherical indenter to evaluate τ_y. The radius of the spherical tip, R, was estimated by a Hertzian contact analysis [13] of indentations on fused quartz and was determined as 5.75 μm.

Figure 1 shows representative microstructures of the as-extruded sample and the edges of the disks processed by HPT for $N = 1/4$, 1/2 and 2 turns. There is a noticeable change in microstructure through HPT processing. Thus, the as-extruded condition in Figure 1a consists of a bimodal microstructure with a large area fraction (>50%) of coarse grains with sizes of ~25 μm surrounded by some fine grains with sizes of ~4–5 μm. After processing through 1/4 turn (Fig. 1b), both the fraction and size of the coarse grains was significantly reduced to ~35% and ~20 μm, respectively, and the fine grains were refined to ~2–3 μm with an increased area fraction of ~65%. After 1/2 turn (Fig. 1c), the coarse grains remained unchanged at ~20 μm but the fine grains occupied a high area fraction of ~75% with an average size of ~1.0–1.5 μm. Thereafter, the microstructure remained constant with further increase in N and the microstructural features after 2 turns were similar to those at 1/2 turn as shown in Figure 1d, thereby demonstrating a reasonable level of microstructural saturation up to at least 2 turns.

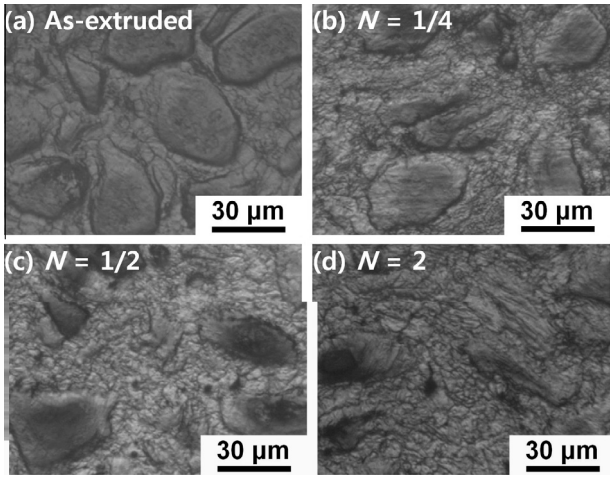

Figure 1. Representative optical micrographs taken at the edges of the ZK60 disks (a) in the as-extruded condition and after HPT for (b) 1/4, (c) 1/2 and (d) 2 turns.

The microstructural evolution may be explained in terms of dynamic recrystallization (DRX). Thus, although deformation within each coarse grain is insufficient for activating DRX due to the limited active slip systems, the stress concentrations generated at high-angle grain boundaries can trigger DRX leading to the nucleation of new grains preferentially along the original boundaries in a necklace-like pattern with the interiors of the coarse grains remaining unrefined [5]. The bimodal structure introduced after $N = 2$ turns is in agreement with earlier ECAP studies on ZK60 alloys [4,5] and demonstrates that the processed microstructure is essentially dependent upon the initial grain size. In practice, a bimodal grain size distribution is advantageous because of the potential for achieving both high strength and good ductility [14].

The variations in Vickers microhardness vs. distance from the centers are shown in Figure S1 of the online Supplementary material for the as-extruded disk and the processed disks with increasing N. Compared with the as-extruded sample where $Hv \approx 72$, all processed disks exhibit higher Hv throughout their diameters. There is a consistent trend of lower Hv in the centers of the disks and increasing Hv towards the edges where the ε_{eq} is the highest, thereby demonstrating a strain-hardening type of hardness evolution [15]. Although there are distinct scatters in Hv due to the bimodal microstructure, the Hv values are reasonably saturated at points beyond ~2 mm from the centers of all processed disks, and thus there is reasonable microstructural homogeneity around the peripheries of the disks. Accordingly, examinations of m and τ_y were conducted near the disk edges where the gradient in mechanical properties was a minimum and the values of ε_{eq} were the highest.

The values of the nanoindentation hardness H, estimated by the Oliver–Pharr method [16], were obtained at the edge of each disk at four different indentation strain rates from 0.0125 to 0.1 s^{-1} and the results are displayed with increasing N in Figure 2. Also shown are the average Hv values at the edges which were recalculated as the peak load divided by the projected contact area. Although higher values were recorded for H compared to Hv due to the indentation size effect [17], the data sets for H and Hv show a consistent trend which increases rapidly in the early stage of HPT and thereafter saturates towards maximum values. This trend is due to the absence of significant grain

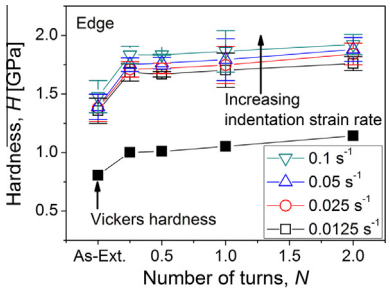

Figure 2. Variations in nanohardness and Vickers microhardness as a function of N: "As-Ext." denotes the as-extruded condition.

refinement after $N = 1/2$ turn as well as the relatively weak Hall–Petch response in Mg alloys [18] which contrasts with typical face-centered cubic (fcc) metals.

Close inspection of Figure 2 shows that H is rate sensitive and increases with the indentation strain rate $\dot{\varepsilon}_i = h^{-1}(dh/dt)$, where h is the indentation depth. The value of the strain-rate sensitivity, m, may be determined at a given strain, ε, and absolute temperature, T, by the expression [19]:

$$m = \left(\frac{\partial \ln \sigma_f}{\partial \ln \dot{\varepsilon}}\right)_{\varepsilon,T} = \left(\frac{\partial \ln(H/C)}{\partial \ln(\beta\dot{\varepsilon}_i)}\right)_{\varepsilon,T}, \quad (1)$$

where the flow stress σ_f is estimated by the Tabor empirical relation of $\sigma_f \approx H/C$ where C is a constraint factor of ~3 for fully plastic deformation [20] and the uniaxial strain rate $\dot{\varepsilon}$ is approximated as $\sim \beta\dot{\varepsilon}_i$. Here, β is taken as ~0.01 based on earlier results [21], but it may vary with the material and loading conditions [21,22]. In the present study, two different methods were applied for estimating m and each calculated value of m was plotted as m vs. N as shown in Figure 3. First, m was evaluated using CSR testing where the nanoindentation was performed at a fixed peak load P_{max} of 50 mN under a constant $\dot{\varepsilon}_i$. As shown in Figure 2, a set of H was obtained for different values of $\dot{\varepsilon}_i$ and then the value of m was calculated using Eq. (1). Second, the m values were estimated by conducting SRJ indentation tests. During a single SRJ test, the sample experiences three different $\dot{\varepsilon}_i$ (0.25, 0.025, 0.0025 s^{-1}), until h reaches a maximum of ~1.9 μm at P_{max}. The values of H were calculated at three different $\dot{\varepsilon}_i$ regimes after these rate changes: further details of SRJ testing are given elsewhere [22]. The essential merit of the SRJ test is that the value of m is obtained from a single indentation which contrasts with the multiple indentations in the CSR tests.

Despite a slight difference in the absolute values of m in Figure 3, such as ~0.048 from SRJ and ~0.043 from CSR at $N = 2$, the overall trend is very similar for these two testing methods. Thus, the estimated m is enhanced significantly through 1/2 turn and thereafter remains reasonably constant with increasing N up to 2 turns. The estimated values of m in this investigation are in good agreement with reported values as summarized in Table S1 of the Supplementary material. It should be noted that the values obtained from uniaxial tensile testing depend upon the strain taken for the flow stress [23].

The mechanism for the rate-dependent plastic deformation may be estimated from the value of the activation volume V^* which is given by [19]:

$$V^* = \sqrt{3}kT\left(\frac{\partial \ln \dot{\varepsilon}}{\partial \sigma_f}\right) = \sqrt{3}kT\left(\frac{\partial \ln(0.01\dot{\varepsilon}_i)}{\partial(H/3)}\right), \quad (2)$$

where k is Boltzmann's constant. Taking $\boldsymbol{b} = 3.2 \times 10^{-10}$ m for Mg [24], the values of V^* were estimated from Eq. (2) for both testing methods and are summarized in Table 1. The values from both methods demonstrate identical trends: V^* decreases in the early stage of HPT through 1/4 turn but saturates to a minimum value with further increase in N. These estimated values of $V^* \approx 10\boldsymbol{b}^3$ are consistent with the reported values for grain boundary sliding (GBS) [25]. Furthermore, the grain boundary diffusivity of Mg is faster by a few orders of magnitude than in fcc metals such as Cu and Ni [24] and there is a high potential for GBS occurring through grain boundary diffusion within the fine-grained regions of the ZK60 alloy even at RT. This conclusion is also consistent with a recent report of GBS at RT in pure Mg [26].

Attention in the present study was also focused on incipient plasticity in the ZK60 alloy after HPT by estimating the shear yield strength, τ_y. When nanoindentation is performed with a spherical indenter, it is possible to predict the elastic response using the Hertzian theory for early contact [13] and the load–displacement (P–h) curves often exhibit sudden bursts of displacement denoted as "pop-ins" [27]. Figure 4 shows representative examples of P–h curves exhibiting pop-ins in the present investigation. The P–h curve obtained at low peak load before the first pop-in (see blue data in the curves) shows that the loading curve is retraced by the unloading curve, indicating purely elastic deformation. Therefore, the "first" pop-in corresponds to the elastic-to-plastic transition at yielding.

Accordingly, the load leading to the pop-in is used to compute τ_{max} representing the maximum shear stress for the onset of plasticity, and thus τ_y, as [13]:

$$\tau_{max} = 0.31\left(\frac{6E_r^2}{\pi^3 R^2}P\right)^{\frac{1}{3}}, \quad (3)$$

where R is the indenter radius and E_r is the reduced modulus. The main plot in Figure 4 summarizes the dependence

Table 1. Summary of the activation volumes.

N	V^* ($\times\boldsymbol{b}^3$)		V_y^* ($\times\boldsymbol{b}^3$)
	CSR test	SRJ test	
As-extruded	9.97	10.22 ± 3.59	0.63
1/4	8.56	8.19 ± 2.23	0.76
1/2	8.16	7.38 ± 1.39	0.78
1	8.36	7.24 ± 1.69	0.76
2	8.19	7.34 ± 1.43	0.78

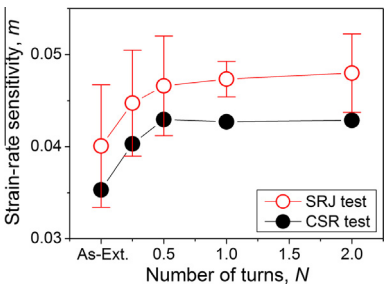

Figure 3. Variations of the strain-rate sensitivity with different levels of torsion straining: data were obtained through CSR and SRJ testing.

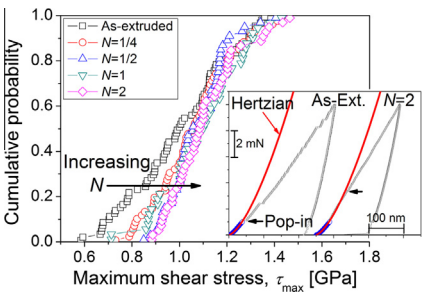

Figure 4. Cumulative probability distribution of τ_{max} with increasing N where the small inset shows representative P–h curve with pop-ins.

of τ_{max} ($=\tau_y$) upon HPT processing by plotting the cumulative probability f vs. τ_{max} for different N. In practice, the average τ_{max} increases to 1.076 ± 0.120 GPa after 1/2 turn and then steadily towards a saturation level of 1.104 ± 0.145 GPa through 2 turns.

The cumulative distribution function, f, of τ_{max} may be described as a function of the instantaneous shear stress beneath the indenter [27,28]:

$$\ln[\ln(1-f)^{-1}] = \left\{ -\frac{\Delta F_y^*}{kT} + \ln\left[\frac{kT\dot{\gamma}_0}{V_y^*(d\tau/dt)}\right]\right\} + \left(\frac{V_y^*}{kT}\right)\tau, \quad (4)$$

where $\dot{\gamma}_0$ is the attempt frequency or frequency of the fundamental mode vibration along the reaction pathway, τ is the applied shear stress and ΔF_y^* and V_y^* are the Helmholtz activation energy and volume of the yielding event, respectively. Therefore, V_y^* can be estimated from the slope of the curve in a $\ln[\ln(1-f)^{-1}]$ vs. τ_{max} plot and these estimated values are summarized in Table 1.

Although a small increase in V_y^* is recorded through 1/4 turn of HPT, all samples exhibit $V_y^* \approx 1\boldsymbol{b}^3$ which corresponds to yielding by heterogeneous dislocation nucleation [28,29]. Two conclusions may be reached by comparing V_y^* for the incipient plasticity of yielding with V^* for the bulk plasticity in Table 1. First, V_y^* ($\sim 1\boldsymbol{b}^3$) is one order of magnitude smaller than V^* ($\sim 10\boldsymbol{b}^3$) and this is consistent with a change in mechanism from heterogeneous dislocation nucleation for the former to GBS for the latter. Second, despite changes in H and m through HPT processing, both V_y^* and V^* remain reasonably constant up to 2 turns, demonstrating that the inherent mechanisms of yielding and bulk plastic deformation remain unchanged through HPT processing. This independence of N is reasonable because the sizes of the highly stressed zones beneath the indenter in the pop-in tests for V_y^* are smaller than the average sizes of the fine grains in all HPT-processed disks, whereas in the CSR and SRJ tests for V^* the stressed zone sizes are larger than the fine grain size of the HPT disks [30]. In addition, the slight but measurable differences in the values of V_y^* and V^* between the samples after extrusion and after HPT are attributed to the presence of a larger fraction of coarse grains in the sample before HPT and the increasing fraction of fine grains after HPT processing

In summary, significant grain refinement was achieved in a ZK60 Mg alloy after processing by HPT and investigations of the processed samples suggest the occurrence of yielding by heterogeneous dislocation nucleation and subsequent flow where GBS is important.

Research at Hanyang University was supported in part by the Human Resources Development program (No. 20134030200360) of the KETEP grant funded by the Korean government (MOTIE) and in part by the NRF grant (No. 2013R1A1A2A10058551) funded by the Korean Government (MSIP). Work at Ajou University was supported by the Basic Science Research Program through NRF funded by MSIP (No. 2012R1A1A1012983). Research in the UK was supported by the European Research Council under ERC Grant Agreement No. 267464-SPDMETALS.

Supplementary data associated with this article can be found, in the online version, at http://dx.doi.org/10.1016/j.scriptamat.2014.09.014.

[1] B.-C. Suh, M.-S. Shim, K.S. Shin, N.J. Kim, Scripta Mater. 84–85 (2014) 1.
[2] R.Z. Valiev, T.G. Langdon, Prog. Mater Sci. 51 (2006) 881.
[3] A.P. Zhilyaev, T.G. Langdon, Prog. Mater Sci. 53 (2008) 893.
[4] R.B. Figueiredo, T.G. Langdon, Mater. Sci. Eng., A 501 (2009) 105.
[5] R.B. Figueiredo, T.G. Langdon, J. Mater. Sci. 45 (2010) 4827.
[6] Y. Huang, R.B. Figueiredo, T. Baudin, F. Brisset, T.G. Langdon, Adv. Eng. Mater. 14 (2012) 1018.
[7] T.G. Langdon, Acta Mater. 61 (2013) 7035.
[8] R.Z. Valiev, Y.V. Ivanisenko, E.F. Rauch, B. Baudelet, Acta Mater. 44 (1996) 4705.
[9] R.B. Figueiredo, T.G. Langdon, Mater. Sci. Eng., A 528 (2011) 4500.
[10] S.A. Torbati-Sarraf, T.G. Langdon, J. Alloys Compd. 613 (2014) 357.
[11] C. Bettles, M. Gibson, JOM 57 (5) (2005) 46.
[12] R.B. Figueiredo, P.R. Cetlin, T.G. Langdon, Mater. Sci. Eng. A528 (2011) 8198.
[13] K.L. Johnson, Contact Mechanics, Cambridge University Press, Cambridge, 1985.
[14] Y. Wang, M. Chen, F. Zhou, E. Ma, Nature 418 (2002) 912.
[15] M. Kawasaki, B. Ahn, T.G. Langdon, Mater. Sci. Eng. A527 (2010) 7008.
[16] W.C. Oliver, G.M. Pharr, J. Mater. Res. 7 (1992) 1564.
[17] G.M. Pharr, E.G. Herbert, Y. Gao, Annu. Rev. Mater. Res. 40 (2010) 271.
[18] D. Orlov, K.D. Ralston, N. Birbilis, Y. Estrin, Acta Mater. 59 (2011) 6176.
[19] I.-C. Choi, Y.-J. Kim, B. Ahn, M. Kawasaki, T.G. Langdon, J.-I. Jang, Scripta Mater. 75 (2014) 102.
[20] S. Shim, J.-I. Jang, G.M. Pharr, Acta Mater. 56 (2008) 3824.
[21] C.L. Wang, Y.H. Lai, J.C. Huang, T.G. Nieh, Scripta Mater. 62 (2010) 175.
[22] V. Maier, K. Durst, J. Mueller, B. Backes, H.W. Höppel, M. Göken, J. Mater. Res. 26 (2011) 1421.
[23] I.-C. Choi, Y.-J. Kim, Y.M. Wang, U. Ramamurty, J.-I. Jang, Acta Mater. 61 (2013) 7313.
[24] H.J. Frost, M.F. Ashby, Deformation-Mechanism Maps, Pergamon Press, London, 1982.
[25] H. Conrad, Nanotechnology 18 (2007) 325701.
[26] H. Somekawa, T. Mukai, Philos. Mag. Lett. 90 (2010) 883.
[27] I.-C. Choi, Y. Zhao, Y.-J. Kim, B.-G. Yoo, J.-Y. Suh, U. Ramamurty, J.-I. Jang, Acta Mater. 60 (2012) 6862.
[28] C.A. Schuh, A.C. Lund, J. Mater. Res. 19 (2004) 2152.
[29] C.A. Schuh, J.K. Mason, A.C. Lund, Nat. Mater. 4 (2005) 617.
[30] H. Somekawa, C.A. Schuh, Acta Mater. 59 (2011) 7554.